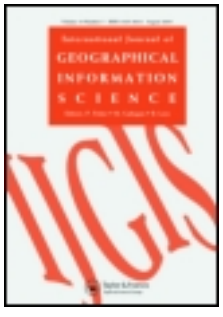

International Journal of Geographical Information Science

Publication details, including instructions for authors and subscription information:
http://www.tandfonline.com/loi/tgis20

Large-scale land cover mapping with the integration of multi-source information based on the Dempster-Shafer theory

Y.H. Ran [a], X. Li [a], L. Lu [a] & Z.Y. Li [b]

[a] Cold and Arid Regions Environmental and Engineering Research Institute, Chinese Academy of Sciences, Lanzhou, China

[b] Institute of Forest Resource Information Techniques, Chinese Academy of Forestry, Beijing, China

Available online: 09 Jan 2012

To cite this article: Y.H. Ran, X. Li, L. Lu & Z.Y. Li (2012): Large-scale land cover mapping with the integration of multi-source information based on the Dempster-Shafer theory, International Journal of Geographical Information Science, DOI:10.1080/13658816.2011.577745

To link to this article: http://dx.doi.org/10.1080/13658816.2011.577745

International Journal of Geographical Information Science
i*First*, 2012, 1–23

Large-scale land cover mapping with the integration of multi-source information based on the Dempster–Shafer theory

Y.H. Ran[a], X. Li[a]*, L. Lu[a] and Z.Y. Li[b]

[a]*Cold and Arid Regions Environmental and Engineering Research Institute, Chinese Academy of Sciences, Lanzhou, China;* [b]*Institute of Forest Resource Information Techniques, Chinese Academy of Forestry, Beijing, China*

(*Received 29 November 2010; final version received 31March 2011*)

Land cover type is a crucial parameter that is required for various land surface models that simulate water and carbon cycles, ecosystem dynamics, and climate change. Many land use/land cover maps used in recent years have been derived from field investigations and remote-sensing observations. However, no land cover map that is derived from a single source (such as satellite observation) properly meets the needs of land surface simulation in China. This article presents a decision-fuse method to produce a higher-accuracy land cover map by combining multi-source local data based on the Dempster–Shafer (D–S) evidence theory. A practical evidence generation scheme was used to integrate multi-source land cover classification information. The basic probability values of the input data were obtained from literature reviews and expert knowledge. A Multi-source Integrated Chinese Land Cover (MICLCover) map was generated by combining multi-source land cover/land use classification maps including a 1:1,000,000 vegetation map, a 1:100,000 land use map for the year 2000, a 1:1,000,000 swamp-wetland map, a glacier map, and a Moderate-Resolution Imaging Spectroradiometer land cover map for China in 2001 (MODIS2001). The merit of this new map is that it uses a common classification system (the International Geosphere-Biosphere Programme (IGBP) land cover classification system), and it has a unified 1 km resolution. The accuracy of the new map was validated by a hybrid procedure. The validation results show great improvement in accuracy for the MICLCover map. The local-scale visual comparison validations for three regions show that the MICLCover map provides more spatial details on land cover at the local scale compared with other popular land cover products. The improvement in accuracy is true for all classes but particularly for cropland, urban, glacier, wetland, and water body classes. Validation by comparison with the China Forestry Scientific Data Center (CFSDC)–Forest Inventory Data (FID) data shows that overall forest accuracies in five provinces increased to between 42.19% and 88.65% for our MICLCover map, while those of the MODIS2001 map increased between 27.77% and 77.89%. The validation all over China shows that the overall accuracy of the MICLCover map is 71%, which is higher than the accuracies of other land cover maps. This map therefore can be used as an important input for land surface models of China. It has the potential to improve the modeling accuracy of land surface processes as well as to support other aspects of scientific land surface investigations in China.

Keywords: land cover; data fusion; remote sensing; land surface modeling; China

*Corresponding author. Email: lixin@lzb.ac.cn

ISSN 1365-8816 print/ISSN 1362-3087 online

http://dx.doi.org/10.1080/13658816.2011.577745
http://www.tandfonline.com

1. Introduction

Land cover plays a significant role in earth system science and reflects the influence of human activities and environmental change (IGBP 1990, DeFries *et al.* 1995, Sellers *et al.* 1997, Bonan *et al.* 2002, 2003, Aspinall and Justice 2003). These changes in land cover affect the function and structure of land surface processes such as energy exchange, the water cycle, the biogeochemical cycle, and vegetation productivity (Hederson-Sellers and Wilson 1983, Crutzen and Andreae 1990, Keller *et al.* 1991, Turner *et al.* 1995). Therefore, accurate land cover maps are the foundation for land surface, ecological and hydrological modeling, carbon- and water-cycle studies, and research on global climate change (IGBP 1990, Sellers *et al.* 1997). Many parameters in a land surface model are assigned based on the land cover types; examples are the time-invariant model variables (e.g., vegetation reflectance, canopy top height, canopy base height, root depth, and leaf respiration factor) in the SIB2 (Simple Biosphere Model 2) and the CoLM (Common Land Model) (Sellers *et al.* 1996, Dai *et al.* 2001).

Many global-, continental-, and regional-scale land use/land cover maps have been produced in recent years using remote-sensing data. Among them, four land cover maps are very popular. These are the Version 2 International Geosphere-Biosphere Programme Data and Information System global land cover data set (IGBPDISCover) map (Loveland *et al.* 2000), the land cover map of the University of Maryland (UMd) (Hansen *et al.* 2000), the Global Land Cover map from the European Commission Joint Research Centre (GLC2000) (Bartholome and Belward 2005), and the Moderate-Resolution Imaging Spectroradiometer (MODIS) global land cover map products (Friedl *et al.* 2002). Ran *et al.* (2010) evaluated the China portions of the four global land cover maps and concluded that none of the four maps met the needs of land surface simulations of China. For China, a 1:100,000 land use map (Liu 1996, Liu *et al.* 2002, 2003a) and a 1:1,000,000 vegetation map (Hou 2001) are available along with other relevant data. Although they offer important land cover information, these data have different purposes and classification systems that are not necessarily compatible with the needs of land surface modeling. Therefore, this study undertakes the important task of determining how to fuse these data into new and more accurate land cover maps with a common classification system that can be used in land surface models.

Dempster–Shafer (D–S) evidence theory (Dempster 1967, Shafer 1976) is a method of inexact reasoning. It is based on the recognition that the knowledge and information (such as land cover classifications) used in decision-making is often uncertain, incomplete, and imprecise. Recently, a new development of D–S evidence theory was proposed in computer science (Wu *et al.* 2002, Lu and Ye 2005). This new development can reduce some of the fuzzy and contradictory evidence used in data analysis. Evidence theory has been used in a variety of land cover case studies (Peddle 1995, Comber *et al.* 2004, Soh *et al.* 2004, Cohen and Shoshany 2005, Cayuela *et al.* 2006, Sun *et al.* 2008, Cao *et al.* 2009), but it has not been widely applied to large areas and with integrated land cover classification information (i.e., discrete information).

In this article, the primary objective of the land cover mapping is to facilitate the extraction of biogeophysical information from land cover for use in regional and global modeling studies. Thus, the specific land cover classification units must not only be discernible (and with high accuracy) from remotely sensed and ancillary data but also be directly related to the physical characteristics of the surface (primarily to the surface vegetation). A set of 17 such global land cover classes has been developed specifically for this purpose by the IGBPDIS in conjunction with the IGBP Core Projects (Belward 1996). The IGBP classification system is widely accepted and applied to the classification of global or regional land cover maps and is also used in land surface process modeling.

This article aims to produce a highly accurate land cover map of China with a common classification system (i.e., the IGBP classification system) by developing a simple and practical decision-fuse method based on the D–S evidence theory for fusing multi-source land cover classification information over China. The article is organized as follows. Section 1 discusses the existing land cover maps of China and the rationale and objectives of the article. Section 2 introduces the input and reference data, and Section 3 presents the method of fusing the data along with data processing. Section 4 presents the results, along with an evaluation of the uncertainty and accuracy of the resultant map as compared to other land cover maps, and a validation of the map using the reference data introduced in Section 2. Section 5 discusses the article's findings and provides conclusions.

2. Materials

The IGBP land cover classification scheme is treated in this article as a common classification system. This set of land cover types includes 11 categories of natural vegetation broken down by life form, 3 classes of developed and mosaic lands, and 3 classes of nonvegetated lands. The classification system is presented in Table 1.

Five relevant land cover data sets were used in this study. They include a 1 km land use map of China at a 1:100,000 scale from the year 2000 land use database (Liu *et al.* 2002), a 1:1,000,000 vegetation map of China (Hou 2001), a 1:100,000 glacier distribution map (Wu and Li 2004, Shi 2005), a 1:1,000,000 swamp map of China (Zhang 2002), and the MODIS global 1 km land cover classification product for 2001 (MODIS2001) (Hodges *et al.* 2001, Friedl *et al.* 2002). These five data sets were converted to raster format with a common spatial resolution (1 km) and were integrated to produce a new land cover map with the IGBP classification system.

The classification systems of the five data sets are not compatible with commonly used land surface models. These data sets contain unique characteristics but also complement each other for use in the IGBP land cover scheme. The 1 km land use map of China was derived from the 1:100,000 land use database; its 1 km grid was geocoded using the greatest-area method (i.e., if a cell has more than one possible code – i.e., it contains two or more polygons – the code of the polygon with the greatest area in the cell is

Table 1. The IGBP land cover classification system (Belward 1996).

S.No.	Class name
1	Evergreen needleleaf forest
2	Evergreen broadleaf forest
3	Deciduous needleleaf forest
4	Deciduous broadleaf forest
5	Mixed forest
6	Closed shrublands
7	Open shrublands
8	Woody savannas
9	Savannas
10	Grasslands
11	Permanent wetlands
12	Croplands
13	Urban and built-up lands
14	Cropland/natural vegetation mosaics
15	Snow and ice
16	Barren or sparsely vegetated lands
17	Bodies of water

used). The 1:100,000 land use database was derived by manual interpretation of Landsat multispectral scanner (MSS), thematic mapper (TM), and enhanced TM (ETM) images. The boundaries of the land use types were delineated based on the interpreters' understanding of spectral reflectance, texture, and terrain, along with other information about land objects. Subsequently, the attributes (labels) of the polygons were labeled to produce the digital map, and the vector digital maps were edited and compiled (Liu 1996). The database was validated by intensive field surveys including an accumulated survey length of 75,271 km across China. The overall accuracy of the land use map is 95% for 25 land use classes (Liu *et al.* 2005). However, the land use data are based on a tiered classification system that lacks information about vegetation types and seasonal characteristics, and they could not be used in land surface models. The vegetation map of China supplies information on vegetation types and seasonal characteristics that is lacking in the land use data. The vegetation map of China was developed based on many forest inventories and vegetation survey data that were collected over half century. These data were combined with airborne and satellite remote-sensing images and data from geology, soil, and climate studies. Therefore, the vegetation map of China reflects detailed distributions of vegetation and includes horizontal and vertical zones of 11 vegetation groups, 54 vegetation types, and 796 biome and sub-biome units (Hou 2001). The MODIS2001 map provides consistent global land cover classification information. The 1:100,000 glacier distribution map and the 1:1,000,000 swamp map offer accurate information on the distribution of glaciers and permanent wetlands in China.

The Forest Inventory Data (FID) at the province scale from the China Forestry Scientific Data Center (CFSDC) (http://www.cfsdc.org) were developed around 2000 and were used as reference data to validate the results of this study. The CFSDC-FID data were the results of the most comprehensive forest-resource inventory in China (Lei *et al.* 2009). They were produced by the Chinese Academy of Forestry, State Forestry Administration of China (CAF-SFA) by integrating the National Forest Continues Inventory and the Forest Management Inventory. The merits of the two inventories are that they combine high-resolution satellite data (e.g., TM/ETM images) with field surveys at the county level. Additional technical details can be found in the references (SFA 2004). The reason to choose the FID data as reference data is that it identifies forests in China with the highest leaf-form accuracy (i.e., the data provide high-accuracy classifications of needleleaf forests, broadleaf forests, mixed forests, and shrublands). In addition, this is the most authoritative forest distribution map in China.

3. Methods

The D–S theory was used to combine the five sources of evidence. This method is an extension of Bayesian probability theory and allows for the quantification and management of data uncertainty (Gordon and Shortliffe 1985, Lee *et al.* 1987). The basic assumptions of D–S theory are that gaps exist in the body of knowledge and that belief in a hypothesis is not necessarily the complement of belief in its negation. In land cover mapping, D–S theory offers several advantages over traditional classification methods (such as a maximum-likelihood classifier). It has the ability to handle the data that may violate the Gaussian assumption and the data from any number of sources at any scale of measurement (Sun *et al.* 2008).

3.1. The D–S evidence theory

The basic concept of evidence theory is the frame of discernment, denoted by θ. The selection of θ depends on the known knowledge and the level of understanding as well

as what we want to know. In image classification, θ corresponds to the categories of the classification system. For example, the IGBP classification system is a set of 17 elements corresponding to the 17 IGBP land cover types.

The computing elements of D–S theory are the power set 2^{θ}. Note that there is a one-to-one correspondence between the elements of 2^{θ} and the subsets of θ. A singleton set is one with only one class. The degree of belief in the evidence from a source (e.g., a land use class) in support of an IGBP class is referred to as the mass (m) committed to that class. The amount of mass is often referred to as an evidence measure. A mass can be expressed as a mass function that maps each element of the power set into a real number from 0 to 1, with a larger value indicating a higher level of 'belief' that expresses the degree to which a pixel belongs to a class. A mass function meets the following conditions:

$$\begin{cases} m(\phi) = 0 \\ \sum\limits_{A \subseteq 2^{\theta}} m(A) = 1 \end{cases} \tag{1}$$

where ϕ is the null set or an empty set and $m(A)$ is a basic probability assignment (BPA) that represents the support for every subset, A. In this study, the subjects of interest are singleton sets or individual classes; therefore, it is necessary to use θ instead of 2^{θ}.

3.2. Generating evidence for each IGBP class

The five land cover data sets were converted to evidence and were then fused according to D–S rules of evidence combination. Transforming input data into evidence (or basic belief) is a critical step in generating evidence (Peddle 1995). The D–S rule of evidence combination determines the final degree of belief in a hypothesis class through combining the basic beliefs. Commonly, two methods are used to assign the basic probability, including the BPA function and expert knowledge. In this study, the discrete variable (i.e., land cover type) was treated as an input data, and it is difficult to determine a function representing the support for real classification. Therefore, the evidence, or the degree of support to each IGBP class from each data source, includes two parts:

$$M_{i,j} = E_{i,j} \times C_{i,j} \tag{2}$$

where E is the data accuracy represented by the proportional error and based on the validation or evaluation of each input data from other research, C is the correlation coefficient between each class of input data and the class from the IGBP classes, the subscript i is the input data number, and the subscript j is the IGBP class number as described in Section 2.

The parameter E was obtained from literature reviews (Hou 2001, Zhang 2002, Liu *et al.* 2003a, Wu and Li 2004). The accuracy of all input data, including the 1 km land use map, the vegetation map, the glacier distribution map, and the swamp map, but with the exception of the MODIS2001 map, was unified at 95%. The four input data sources represent an accumulation of a large volume of research results over many years in China; they are now widely accepted in the scientific community as highly accurate data sets. However, the determinate method of accuracy of the MODIS2001 was different and was identified with a modified evaluation result by Ran *et al.* (2010).

The parameter C defines the relationship between the input-data class and the IGBP class; in this study, it was identified through expert knowledge. The correlation coefficients between the vegetation classes and the IGBP classes were determined by the relationships (shown in Table 2) between Chinese vegetation types and IGBP classes. These correlations are explicit for some types but are ambiguous for others. For example, the vegetation

Table 2. The correlation coefficients between the China vegetation classes and the IGBP land cover classes.

Vegetation type	1	2	3	4	5	6	7	8	9	10	11	12	14	16
Needleleaf forests in cold-temperate zones and on mountains in temperate zones	0.5		0.5											
Needleleaf forests in temperate zones	0.6		0.4											
Needleleaf forests in subtropical zones	1.0													
Needleleaf forests in tropical zones	1.0													
Needleleaf forests on mountains in subtropical and tropical zones	1.0													
Needleleaf and deciduous broadleaf mixed forests in temperate zones					1.0									
Needleleaf, evergreen and deciduous broadleaf mixed forests on mountains in subtropical zones					1.0									
Broadleaf deciduous forests in temperate zones				1.0										
Microphyllous deciduous woodlands in temperate zones				1.0										
Broadleaf deciduous forests in subtropical zones				1.0										
Broadleaf evergreen and deciduous mixed forests in subtropical zones					1.0									
Broadleaf evergreen forests in subtropical zones		1.0												
Sclerophyllous broadleaf evergreen forests in subtropical zones		1.0												
Tropical monsoon forests		1.0												
Tropical rain forests		1.0												
Bamboo forests and scrubs in subtropical and tropical zones		1.0												
Deciduous scrubs in temperate zones						0.4	0.6							
Broadleaf evergreen and deciduous scrubs in subtropical and tropical zones						1.0								
Broadleaf evergreen succulent scrub and dwarf forests on coral islands in tropical zones		0.5				0.5								

Evergreen xeromorphic succulent thorny scrubs in subtropical and tropical zones			1.0						
Subalpine broadleaf deciduous scrubs			1.0						
Subalpine sclerophyllous broadleaf evergreen scrubs			1.0						
Subalpine needleleaf evergreen scrubs	0.2		0.8						
Dwarf semi-arborous deserts					0.5				0.5
Shrub deserts				0.5					0.5
Steppe shrub deserts				0.3	0.3				0.4
Semi-shrub and dwarf semi-shrub deserts				0.5					0.5
Succulent halophytic dwarf semi-shrub deserts				0.5					0.5
Annual herb deserts						0.5			0.5
Cushion nano-semi-shrub high-cold deserts				0.5					0.5
Temperate grass and forb meadow steppes						1.0			
Temperate tufted grass steppes						1.0			
Temperate tufted low grass, nano-semi-shrub desert steppes				0.5		0.5			
Grass and *Carex* spp. high-cold steppes						1.0			
Temperate grasslands			0.2			0.8			
Subtropical and tropical grasslands			0.3			0.7			
Grass and forb meadows						1.0			
Grass, *Carex*, and forb swamp meadows						1.0			
Grass and forb halophytic meadows						1.0			
Kobresia spp. and forb high-cold meadows						1.0			
Cold-temperate and temperate marshes							1.0		
Subtropical and tropical marshes							1.0		
Tropical mangroves			1.0						
High-cold marshes							1.0		
Alpine tundra				0.5		0.5			
Alpine cushion vegetation						1.0			
Alpine sparse vegetation				0.5		0.5			
One-year one-harvest fields with cold-tolerant crops of short growth duration								1.0	
One-year one-harvest grain fields and cold-tolerant economic crop fields								1.0	

(*Continued*)

Table 2. (*Continued*).

Vegetation type	1	2	3	4	5	6	7	8	9	10	11	12	14	16
One-year one-harvest grain fields and cold-tolerant economic crop fields; deciduous orchards				0.3								0.4	0.3	
Two-year three harvest or one-year two-harvest grain fields and deciduous orchards				0.3								0.4	0.3	
One-year two-harvest grain fields; evergreen and deciduous orchards; economic tree plantations		0.1		0.1								0.4	0.4	
One-year two-harvest or three-harvest grain fields; evergreen orchards and subtropical economic tree plantations		0.3										0.4	0.3	
One-year three-harvest grain fields; tropical evergreen orchards and economic tree plantations		0.3										0.4	0.3	
No vegetation														1.0

Note: All empty cells denote zeros.

type 'broadleaf deciduous forests in a temperate zone' has an explicit correlation with IGBP class 4, 'deciduous broadleaf forest,' and the correlation coefficient was assigned as 1. The vegetation type 'needleleaf forests in a cold-temperate zone and on mountains in a temperate zone' does not have a clearly corresponding class; using the information from evergreen and deciduous types, we assigned this vegetation type to IGBP class 1 (i.e., evergreen needleleaf forest) and IGBP class 3 (i.e., deciduous broadleaf forest) with correlation values of 0.5 in each case. In this process, the opinions of vegetation experts played an important role.

The correlation coefficients between the Chinese land use classes and the IGBP classes were also identified (Table 3). As is the case for the vegetation types, this correlation is explicit for some types but is ambiguous for others. For example, the definition of paddy land and dryland in the Chinese land use map is explicit and corresponds to the cropland class definition in the IGBP, which results in a correlation coefficient of 1. As defined in the China land-source classification system, shrublands are lands covered by trees less than 2 m high and with a canopy cover of >40%. This class is related to closed shrublands (6) and open shrublands (7) in the IGBP classification system. However, the definition of canopy cover is closer to closed shrublands than it is to open shrublands; thus, the correlation coefficients between shrublands in the China land-source classification system and closed shrublands and open shrublands in the IGBP classification system were assigned as 0.6 and 0.4, respectively. Most correlation coefficients were assigned using these methods, with the exceptions of 'forest' and 'other forest' in the China land-source classification

Table 3. The correlation coefficients between the Chinese land use classes and the IGBP land cover classes.

Classes	1	2	3	4	5	6	7	8	9	10	11	12	13	15	16	17
Paddy lands												1.0				
Drylands												1.0				
Forest	0.6	0.6	0.6	0.6	0.6											
Shrublands						0.63	0.42									
Woods							0.53	0.53								
Other forest	0.53	0.53	0.53	0.53	0.53											
Dense grass										1.0						
Moderate grass										1.0						
Sparse grass										0.84					0.21	
Streams and rivers																1.0
Lakes																1.0
Reservoirs and ponds																1.0
Permanent ice and snow														1.0		
Beaches and shores																1.0
Bottomlands																1.0
Urban built-up lands													1.0			
Rural settlements													1.0			
Other built-up lands													1.0			
Sandy lands															1.0	
Gobi															1.0	
Salina															1.0	
Swamplands											1.0					
Bare soil															1.0	
Bare rock															1.0	
Other										1.0					0.63	

Note: All empty cells denote zeros.

system. The forest and other forest classes are arbor forest classes; however, they do not concretely specify forest-type information. This provides an accurate boundary for forest; therefore, we assigned a correlation coefficient of 0.6 between forest in the China land-source classification system and evergreen needleleaf forest (1), evergreen broadleaf forest (2), deciduous needleleaf forest (3), deciduous broadleaf forest (4) and mixed forest (5), and a correlation coefficient of 0.5 between other forest in the China land-source classification system and evergreen needleleaf forest (1), evergreen broadleaf forest (2), deciduous needleleaf forest (3), deciduous broadleaf forest (4), and mixed forest (5). Uncertainties do exist in this process, but they are acceptable.

The glacier distribution map depicts IGBP class 15 (snow and ice). The swamp map represents IGBP class 11 (permanent wetlands). The classes from the MODIS2001 use the same IGBP classification system, so the C correlation coefficient is equal to 1. The final level of belief in MODIS2001 is shown in Table 4.

3.3. Combining all the evidence

In general, the basic belief (or evidence) is represented by the mass function. The mass function generates a basic level of belief for each evidence source for a hypothetical class, and then the system of combination is used to combine these basic beliefs to generate a total degree of belief for the hypothetical class. The D–S theory uses an orthogonal sum ($\oplus$) to compute a total belief degree using this equation:

$$m_1 \oplus m_2\,(Z) = \frac{\sum\limits_{X \cap Y = Z} m_1\,(X)\, m_2\,(Y)}{1 - k} \tag{3}$$

where Z is an IGBP class label and X and Y are input data labels. The sum extends over all class labels whose intersection is $X \cap Y = Z$. The set of intersections represents common class labels of evidence. The values of $m_{1 \oplus} m_2(Z)$ are used to determine the combined mass and then assigned to a set of class labels, Z.

The parameter k is a normalization constant. It corrects for any mass that is committed to the empty set (Φ), and it has the form:

$$k = \sum_{X \cap Y = \phi} m_1(X)\, m_2(Y) \tag{4}$$

where k indicates the extent of conflict between the two sources considered (Shafer 1976), $k = 0$ indicates complete compatibility, and k=1 indicates complete contradiction. The value of k between 0 and 1 indicates partial compatibility.

The above equations provide a method to combine two BPA functions, but they can be used with any number of BPA functions by repeating the application of Equations (3) and (4). The implementation of combined evidence is carried out in the belief module of the IDRISI software version 14.01, a GIS and remote-sensing image-processing tool

Table 4. The basic probability values for the MODIS land cover product.

1	2	3	4	5	6	7	8	9	10	11	12	13	14	15	16	17
0.5	0.5	0.5	0.5	0.5	0.45	0.45	0.5	0.45	0.45	0.1	0.54	0.1	0.4	0.6	0.6	0.6

developed by Clark Labs (Worcester, MA), USA. The technical details can be found in Ronald (2003).

3.4. Making classification decisions

The D–S theory provides three functions to describe the degree of belief, degree of plausibility, and belief interval for a hypothesis class. The belief function (Bel) is the total degree of belief of a set and all its subsets. It is defined as

$$\mathrm{Bel}\,(A) = \sum_{B \subseteq A} m\,(B) \tag{5}$$

where B represents any subset of a set A.

The plausibility function (Pl) is defined as the degree to which the evidence fails to reject a hypothesis class, A. It is calculated as 1 minus the support for all other hypotheses (Shafer 1976):

$$\mathrm{Pl}\,(A) = 1 - \mathrm{Bel}\left(\overline{A}\right) \tag{6}$$

The belief function defines the lower boundary of the support committed to an IGBP class, while the plausibility function defines an upper boundary, and the range [Bel, Pl] is referred to as a belief interval or an interval of uncertainty. In this study, the decision rule was based on maximum support, where the class with the greatest support (i.e., the maximum total belief) was assigned to the pixel. The interval of uncertainty for each pixel was also given.

3.5. Accuracy evaluation

In this study, the accuracy of the result map was validated using the following procedures. First, it was validated through visual comparison at local scales; subsequently, detailed and quantified validations for the forests in five provinces were performed using CFSDC-FID data. In the third step, a complete validation over China was carried out based on the ground-truth samples of land cover data obtained from the ChinaFlux sites, the Monsoon Asia Integrated Regional Study (MAIRS) sites, and the high-resolution images from the Google Earth.

In addition, confusion matrices were used to evaluate the accuracy of the forest class with a reference to the CFSDC-FID data. A confusion matrix reports four accuracy measures: producer's accuracy, user's accuracy, overall accuracy, and the kappa coefficient (Jensen 1996, Rahman and Saha 2008). The producer's accuracy is a measure of the accuracy of a particular classification scheme. It shows what percentage of a particular ground class was correctly classified. The user's accuracy is a measure of the reliability of an output map generated from a classification scheme. It is a statistic that can tell the user of the map what percentage of a class corresponds to the ground-truth. The difference between the producer's accuracy and the user's accuracy indicates the direction and degree of error for all areas (Zhu *et al.* 2007). The overall accuracy is the percentage of correctly classified pixels. The kappa coefficient is a statistical measure of the agreement (beyond chance) between two maps (e.g., the output classification map and the ground-truth map).

4. Results and discussion

Using the method proposed in this article, a Multi-source Integrated Chinese Land Cover (MICLCover) map was generated by a decision rule based on maximum support (Figure 1). To analyze the characteristics of the result map, we compared the area of each land cover class of MICLCover map with other two popular land cover maps, that is, the IGBPDISCover and MODIS2001 map. The overall areas for each land cover class of the MICLCover map, the MODIS2001, and the IGBPDISCover maps are shown in Table 5. Note the marked increases in the areas of forests, grasslands, permanent wetlands, croplands, urban and built-up lands, snow and ice, and bodies of water in the MICLCover map and the corresponding decreases in shrublands, woody savannas, and cropland/natural vegetation mosaics. The degree of belief in these increases depends on the high degree of support from the input data. In addition, significant differences are to be expected because the MODIS2001 and IGBPDISCover maps were constructed from remote-sensing data and are not good at recognizing dispersive and small targets. The decrease of woody savanna and cropland/natural vegetation mosaics is due to the lower degree of support by MODIS2001 map.

4.1. Visual comparison at three local plots

Three plots at a local scale were selected to evaluate the differences among the MICLCover, IGBPDISCover, and MODIS2001 maps. The general pattern of the land cover distribution in each plot appears similar, but the details are different (Figure 2). The MICLCover map provides the highest level of details on the land cover patterns for the three plots. Region A shows an area of the Heihe River Basin. Many field experiments have been performed

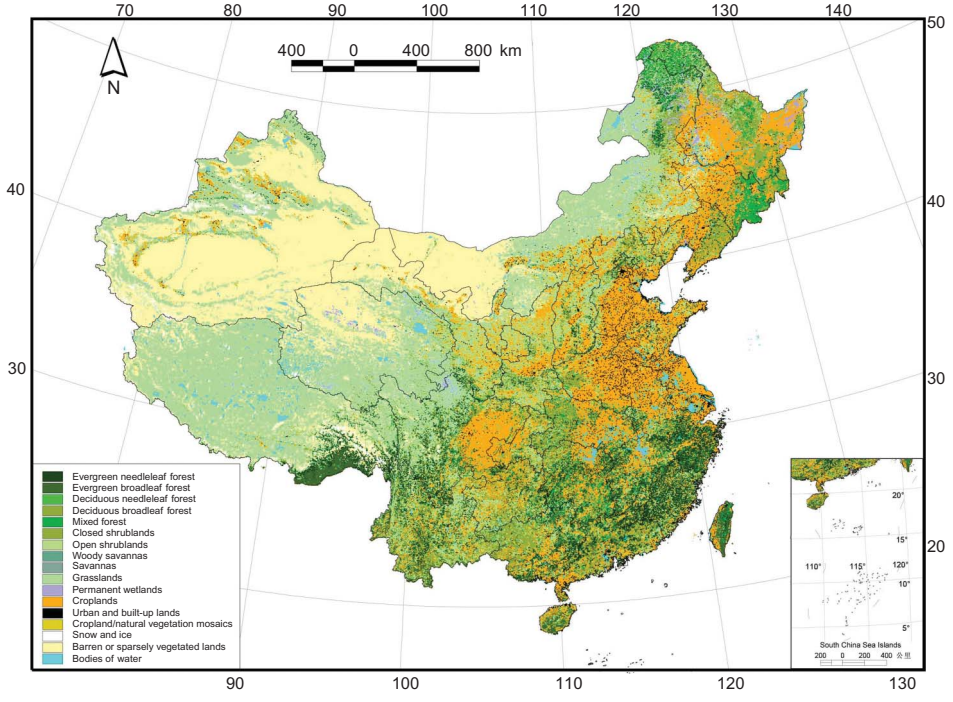

Figure 1. The MICLCover map generated by combining multi-source data in China.

Table 5. The overall area of each IGBP class in the MICLCover, MODIS2001, and IGBPDISCover land cover maps, respectively.

S.No.	Class name	Area (km^2)		
		MICLCover	MODIS2001	IGBPDISCover
1	Evergreen needleleaf forest	543,014	144,935	131,975
2	Evergreen broadleaf forest	249,524	195,959	69,562
3	Deciduous needleleaf forest	11,649	17,892	24,152
4	Deciduous broadleaf forest	317,800	161,746	282,136
5	Mixed forest	231,624	972,482	594,882
6	Closed shrublands	497,813	84,760	282,505
7	Open shrublands	55,112	1,203,542	1,581,434
8	Woody savannas	26,227	476,648	380,349
9	Savannas	110	156,601	39,637
10	Grasslands	3,024,633	1,713,050	1,825,679
11	Permanent wetlands	102,902	12,323	5016
12	Croplands	1,948,136	1,803,962	1,772,116
13	Urban and built-up lands	153,451	93,444	7593
14	Cropland/natural vegetation mosaics	18,904	189,016	942,048
15	Snow and ice	73,856	18,426	13,027
16	Barren or sparsely vegetated lands	2,054,279	2,135,107	1,400,653
17	Bodies of water	211,127	107,649	129,805

in this region by scientific researchers (e.g., the Heihe River Basin Field Experiment in 1990 and the Watershed Allied Telemetry Experimental Research in 2008) (Hu *et al.* 1994, Wang 1999, Li *et al.* 2009). Field-based investigations show that the wider distribution of grassland in the IGBPDISCover map, as compared to the other two maps, is incorrect. The areas in the center of the plot are the Jinta and Zhangye oases where the cropland and the urban and built-up lands are dominant. Region B shows an area in the Qiqihar city of northeast China. According to the CFSDC-FID, there should be no forested lands in this area and according to the field investigation Qiqihar wetland is located here. This shows that the distribution pattern of land cover types in the MICLCover map is more accurate. A similar situation occurs in Region C. The area in the center of Region C is the boundary area of the Dabie Mountains, which are located in the Anhui, Henan, and Hubei provinces. The Forest National Nature Reserve of Dabie Mountains is located in the Region C. According to an investigation by the Forest National Nature Reserve, abundant forest types (most of them are evergreen needleleaf forests) are distributed continuously in this region. Figure 2 shows that the large area of evergreen needleleaf forest was misclassified as woody savannas and cropland/natural vegetation mosaic in the IGBPDISCover map, or as mixed forest in the MODIS2001, but that the MICLCover map represents the forest distribution very well. In addition, the classifications of urban and built-up lands were improved for the three regions in the MICLCover map. The rural settlements (a very important part of the urban and built-up lands) were successfully combined into the MICLCover map from a land use database that was derived from a high-resolution remote sensing and field survey. The MICLCover map shows that the rural settlements are widely distributed in many agricultural areas in China. Most of the rural settlements cannot be discriminated in the IGBPDISCover and MODIS2001 products because the data sources of these two land cover products are Advanced Very High Resolution Radiometer (AVHRR) and MODIS, both of which have coarse resolutions.

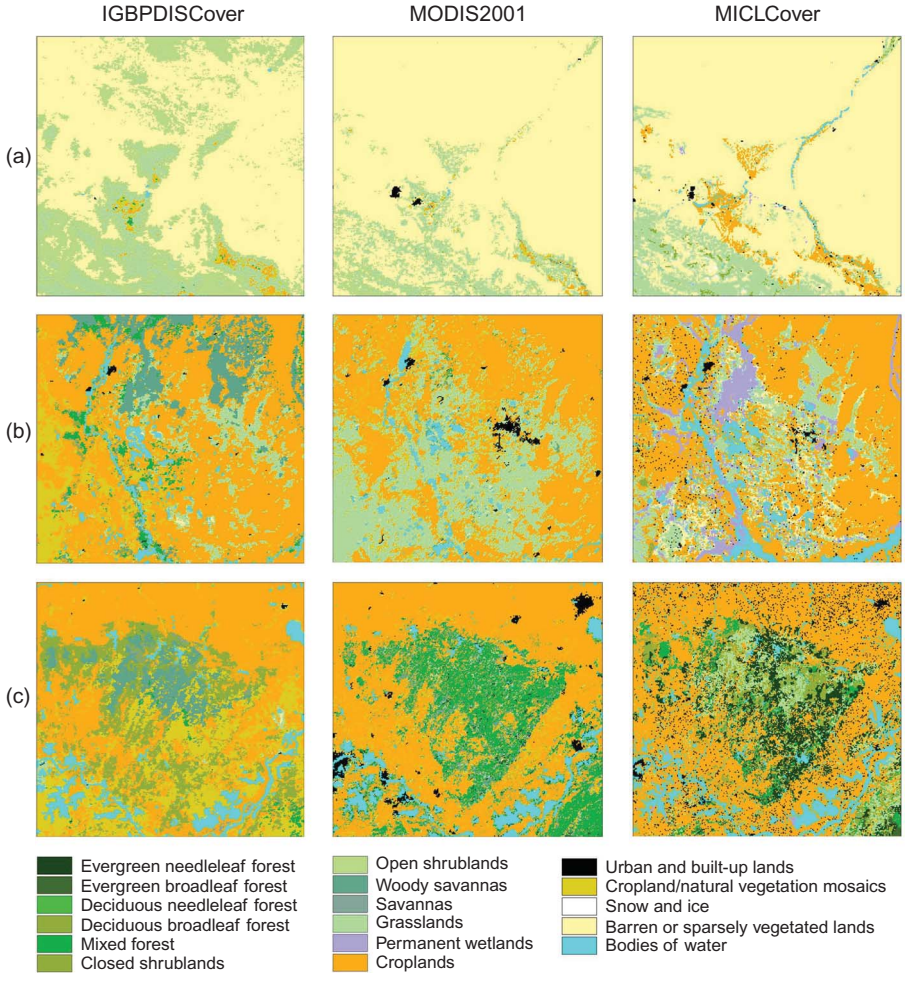

Figure 2. Three local areas depicting the general differences among the three land cover maps. (a) Region A is an area in Northwestern China centered at 99.1234°E and 40.077°N. (b) Region B is an area in Northeastern China centered at 124.602°E and 46.556°N. (c) Region C is an area in the junction between Anhui and Hubei provinces centered at 115.916°E and 30.9643°N.

4.2. Validation of the forest class using CFSDC-FID reference data

According to our evaluation of four remote-sensing-based global land cover products over China (Ran *et al.* 2010), the forest classes have the largest uncertainty. In addition, it is one of the most important classes for land surface modeling. Therefore, we compared the resultant map with the CFSDC-FID data, which are currently available for four forest types within five provinces.

4.2.1. The improvement of percent area for the forest classes

The MICLCover map was compared on a pixel-by-pixel basis with the CFSDC-FID data for four forest types, including needleleaf forest, broadleaf forest, mixed forest, and shrubland, in four regions (five provinces) that are evenly distributed in China. Table 6 shows

Table 6. Percent area of each forest class in the CFSDC-FID data, MODIS2001 land cover product, and MICLCover land cover map for Gansu, Yunnan and Zhejiang provinces and the Northeast region (Heilongjiang and Jilin provinces).

Region	Class	FID	MODIS2001	MICLCover
Gansu	Needleleaf forest	1.67	0.59	1.73
	Broadleaf forest	3.24	0.58	2.52
	Mixed forest	0.77	4.38	0.44
	Shrublands	3.88	13.06	2.96
Yunnan	Needleleaf forest	34.5	1.58	12.82
	Broadleaf forest	18.58	22.97	11.42
	Mixed forest	0.00	24.36	2.67
	Shrublands	11.21	7.32	24.06
Zhejiang	Needleleaf forest	43.21	5.52	40.95
	Broadleaf forest	7.49	4.21	10.33
	Mixed forest	0.00	48.82	5.41
	Shrublands	9.04	2.04	7.04
Northeast	Needleleaf forest	8.19	2.09	4.05
	Broadleaf forest	27.13	8.57	20.75
	Mixed forest	2.84	23.32	11.88
	Shrublands	0.00	3.96	1.30

the percentage area of each forest class in the CFSDC-FID data, the MODIS2001, and the MICLCover for Gansu, Yunnan, and Zhejiang provinces and for the Northeast region (Heilongjiang and Jilin provinces). Figure 3 shows the snapshots of the four regions, indicating the MICLCover map is more similar with CFSDC-FID map than with MODIS2001.

As shown in Table 6, the MICLCover maps are far closer to the CFSDC-FID data in terms of the percentage area of each class. The MICLCover map has a much smaller difference from the CFSDC-FID data than does the MODIS2001 map, with differences of less than 1% for Gansu province, 22% for Yunnan province, 6% for Zhejiang province, and 9% for all classes. The average absolute difference of percentage area between the MICLCover and CFSDC-FID maps is 4.99% for all classes and regions; this is significantly smaller than the difference between the MODIS2001 and the CFSDC-FID maps (14.25%).

4.2.2. The improvement of overall accuracy for forest class

Table 7 shows a comparison between the MODIS2001 and MICLCover maps in terms of classification accuracy and kappa statistics using the CFSDC-FID data as a reference map. Classification accuracies, including the producer's and user's accuracies and the overall accuracy, and the kappa statistics were calculated for the MODIS2001 and our MICLCover maps.

Table 7 shows that the overall accuracies of our MICLCover map are higher than those of the MODIS2001 map for all four regions. Specifically, the overall accuracies of the MODIS2001 map are between 27.77% and 77.89% for the four regions; these values increased to between 42.19% and 88.65% for our MICLCover map. The biggest improvement (from 27.77% to 57.76%) occurred in Zhejiang province. The overall kappa statistic of the MICLCover map also increased for all four regions, with the biggest improvement occurring in Zhejiang (from 0.12 to 0.36).

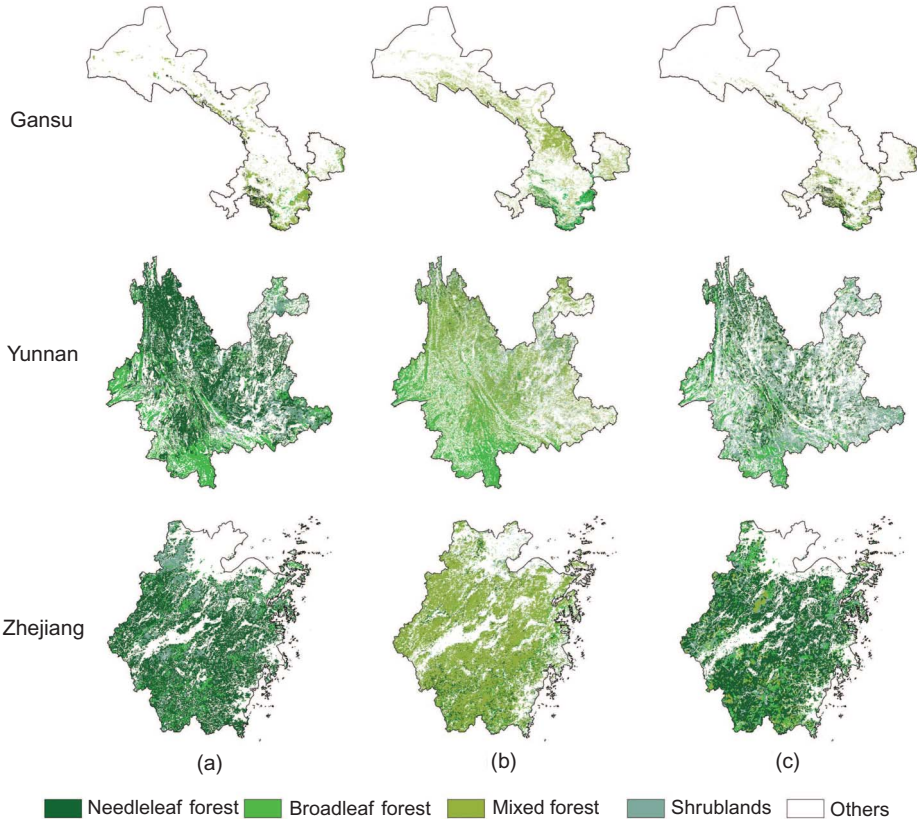

Figure 3. Comparison of the CFSDC-FID data, the MODIS2001 product, and the MICLCover map for Gansu, Yunnan, and Zhejiang provinces: (a) CFSDC-FID data, (b) MODIS2001, and (c) MICLCover map.

At the class level, almost all forest classes were significantly improved. The shrubland class was improved in all four regions. The accuracy of shrubland class in the Northeast region is null for both MODIS2001 and MICLCover maps. The area of shrubland class in reference data is only 8374 km^2, and this class has a fragmented distribution in the Northeast region. All these enhance the difficulty to identify this class. In terms of producer's accuracy, the maximum improvements occurred in Yunnan province. For the shrubland class, the producer's accuracy for the MODIS2001 map is only 8.01%, but for the MICLCover map it increased to 31.46%. For the needleleaf forest class, the two corresponding values are 2.75% and 24.92%, respectively. Another significant improvement occurred in Northeast China. For the broadleaf forest in the region, the producer's accuracy improved from 20.43% to 44.86%. In comparison to the MODIS2001 map, the producer's accuracies for the needleleaf forest class in the MICLCover map increased in Yunnan and Zhejiang provinces and in the Northeast regions but decreased in Gansu province. Because the smaller area of the needleleaf forest class in the MODIS2001 map leads to a relatively higher producer's accuracy, this resulted in a decrease in the accuracy of our MICLCover map in Gansu province for needleleaf forest. For the broadleaf forest class, the producer's accuracies of MICLCover increased in Gansu and Zhejiang provinces and the Northeast regions but decreased in Yunnan province.

Table 7. The confusion matrices of the MICLCover and the MODIS2001 land cover for forest classes using the CFSDC-FID reference data for Gansu, Yunnan and Zhejiang provinces and the Northeast region (Heilongjiang and Jilin provinces).

		Producer's accuracy (%)		User's accuracy (%)	
Province	Class	MODIS2001	MICLCover	MODIS2001	MICLCover
Gansu	Needleleaf forest	32.96	27.32	11.73	28.35
	Broadleaf forest	31.35	35.84	5.64	27.86
	Mixed forest	5.97	6.05	33.78	3.47
	Shrublands	4.79	16.44	16.13	12.56
	Others	94.17	93.95	84.73	95.93
	Overall Accuracy (%)	77.89	88.65		
	Overall kappa	0.14	0.30		
Yunnan	Needleleaf forest	2.75	24.92	59.93	67.03
	Broadleaf forest	46.81	30.81	37.64	50.05
	Mixed forest	0.00	0.00	0.00	0.00
	Shrublands	8.01	31.46	12.25	14.65
	Others	55.69	68.16	45.56	49.68
	Overall Accuracy (%)	30.40	42.19		
	Overall kappa	0.12	0.21		
Zhejiang	Needleleaf forest	56.84	64.17	7.28	60.82
	Broadleaf forest	10.94	15.46	6.19	21.32
	Mixed forest	0.00	0.00	0.00	0.00
	Shrublands	4.83	17.26	1.09	13.44
	Others	62.01	79.03	60.41	71.20
	Overall Accuracy (%)	27.77	57.76		
	Overall kappa	0.12	0.36		
Northeast	Needleleaf forest	14.87	19.82	58.37	40.20
	Broadleaf forest	20.43	44.86	64.76	58.75
	Mixed forest	66.18	47.78	8.06	11.43
	Shrublands	0.00	0.00	0.00	0.00
	Others	82.24	84.14	81.89	83.80
	Overall accuracy (%)	59.50	67.18		
	Overall kappa	0.31	0.41		

The comparative results are different for user's accuracies at the class level. The user's accuracies indicate that all classes improved in the MICLCover map for all four regions except for the mixed forest in Gansu province and the broadleaf forest and needleleaf forest classes in the Northeast regions. This probably can be attributed to the fact that the mixed forest was over-classified in the MODIS2001 map (Figure 3). In all forest and shrubland classes, the difference between the sum of the producer's accuracy and the sum of the user's accuracy is −0.07% for the MICLCover map and −3% for the MODIS2001 map, respectively; this indicates that the overall error of MICLCover map decreased more than the error of the MODIS2001 map did. In addition, this negative difference value shows the direction of error; that is, the areas of most forest and shrubland classes were slightly underestimated in the MICLCover map (also consistent with Table 6).

4.3. Validation all over China using the ground-truth sample data

The validation of the large-scale map for all land cover types in all regions is difficult because of the lack of reference data that can represent a 'true' land cover. Gong (2009)

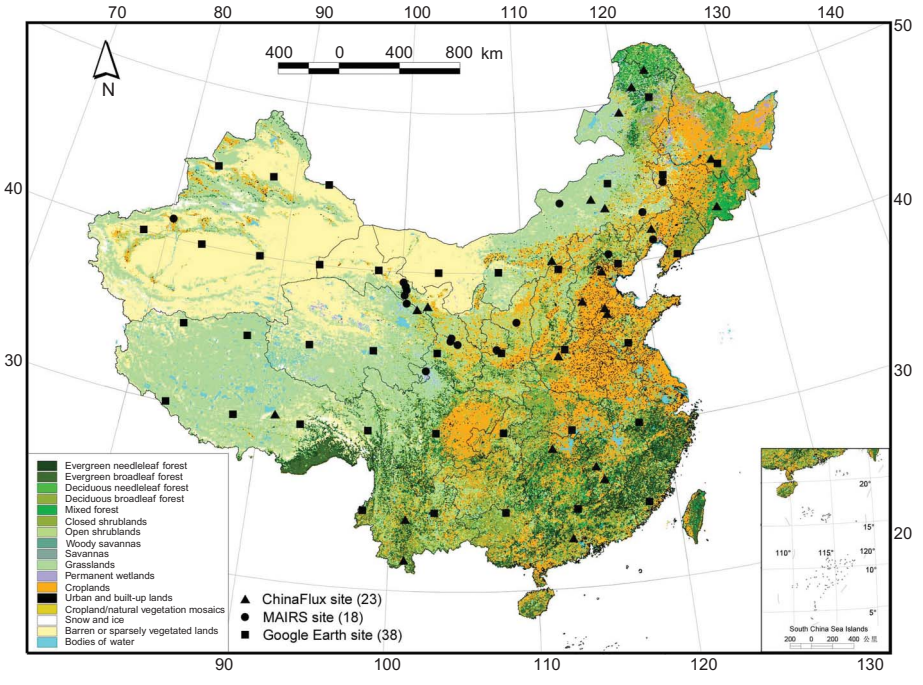

Figure 4. The distribution of ground sample sites for validation all over China.

performed the validation for a global land cover map using the ground-truth sample land cover data from the global flux site. In this article, we applied a similar approach. We used 79 ground-truth sample data points to validate the MICLCover map over China. These data include 23 samples from the ChinaFlux sites (http://www.chinaflux.org), 18 samples from the MAIRS (http://www.mairs-essp.org) sites, and 38 samples from high-resolution images accessed via Google Earth. The distribution of these samples is shown in Figure 4. The results showed that the overall accuracy of the MICLCover map is 71%, which is much higher than the accuracy of the MODIS2001 land cover map (48%).

Obviously, the MICLCover map synthesizes information about the basic appearance of the vegetation (forest, shrubs, and herbaceous vegetation), the leaf attributes (evergreen and deciduous), and the leaf types (broadleaved and coniferous) from the vegetation map. It also extracts bodies of water, urban and built-up lands, and barren areas from the land use map, glacier information from the glacier distribution map, and wetlands from the swamp map. According to Ran *et al.* (2010) and the above analysis, the MICLCover map has a higher accuracy than other land cover maps of China.

4.4. Uncertainty analysis

4.4.1. The spatial distribution of uncertainty

Figure 5 shows that the uncertainties of majority pixels range from 0.0 to 0.1; these pixels are dominated by the barren-land class, which indicates that barren land can be more easily identified than other classes using remote sensing. Only a few pixels have an uncertainty of over 0.4, but the mountainous regions in China have greater levels of uncertainty than

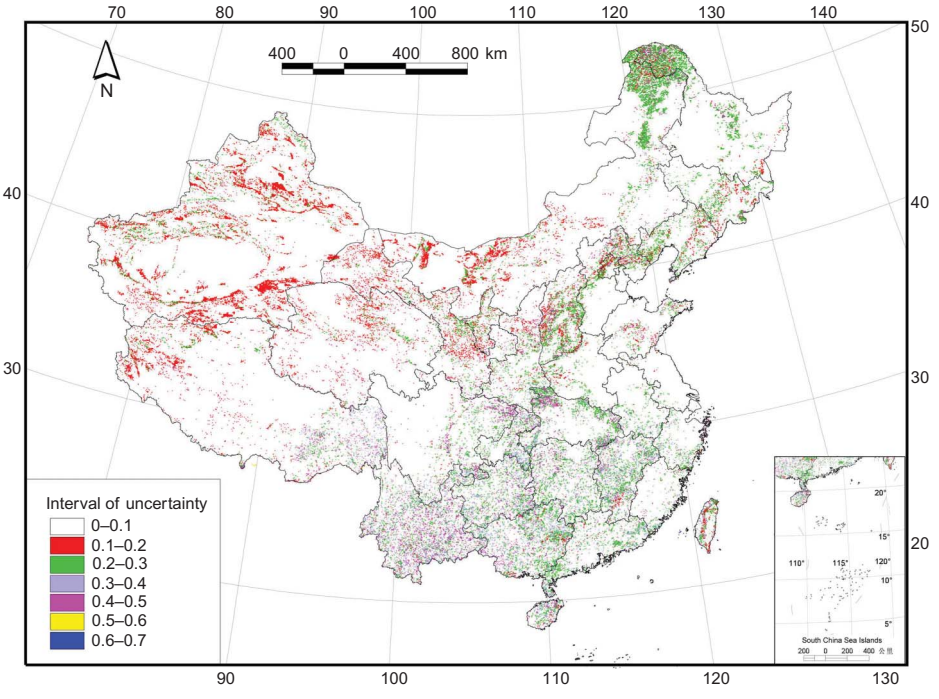

Figure 5. The spatial distribution of the interval of uncertainty for the MICLCover map.

other areas. One possible reason for this is that the land cover is more heterogeneous in mountainous areas due to the complex micro-climates.

4.4.2. The distribution of uncertainty for different land cover types

Table 8 shows the maximum, minimum, mean, and standard deviations of the intervals of uncertainty for each land cover type in the MICLCover map. The intervals of uncertainty of the 17 land cover types can be divided into three levels. The land cover types with the lowest level of the mean intervals of uncertainty include snow and ice, barren or sparsely vegetated lands, permanent wetlands, bodies of water, croplands, grasslands, and urban and built-up lands; the uncertainty of these levels is less than 0.05. This is because the areas of grasslands, croplands, glaciers, snow, barren lands, bodies of water, and urban and built-up lands were combined from the land use map, the swamp map, and the glacier map of China, all of which have high accuracies. The medium level of uncertainty is for the land cover types of evergreen needleleaf forest, evergreen broadleaf forest, deciduous needleleaf forest, deciduous broadleaf forest, mixed forest, closed shrublands, and cropland/natural vegetation mosaics. The mean intervals of uncertainty of these land cover types are relatively low (around 0.17). This can be explained by the fact that the basic appearance of the vegetation (forest, shrubs and herbaceous vegetation), the leaf attributes (evergreen and deciduous), the leaf types (broadleaved and coniferous), and the cropland/natural vegetation mosaic information primarily comes from the vegetation map of China, which is less accurate than the first group of sources. The MODIS2001 was assigned a lower weight and did not significantly affect the uncertainty of these results. The highest level of uncertainty is from the land cover types of savannas, open shrublands, and woody savannas and has a

Table 8. The intervals of uncertainty according to type, with the min, max, range, mean and standard deviation of the results.

Number	Class name	Min	Max	Range	Mean	SD
1	Evergreen needleleaf forest	0.022	0.550	0.529	0.096	0.083
2	Evergreen broadleaf forest	0.022	0.550	0.529	0.134	0.124
3	Deciduous needleleaf forest	0.099	0.500	0.401	0.150	0.062
4	Deciduous broadleaf forest	0.022	0.500	0.479	0.071	0.070
5	Mixed forest	0.022	0.500	0.479	0.176	0.130
6	Closed shrublands	0.024	0.550	0.526	0.155	0.130
7	Open shrublands	0.102	0.550	0.448	0.339	0.120
8	Woody savannas	0.025	0.550	0.525	0.251	0.030
9	Savannas	0.550	0.550	0.000	0.550	0.000
10	Grasslands	0.003	0.640	0.637	0.043	0.068
11	Permanent wetlands	0.000	0.900	0.900	0.035	0.038
12	Croplands	0.002	0.640	0.638	0.041	0.064
13	Urban and built-up lands	0.045	0.900	0.855	0.049	0.014
14	Cropland/natural vegetation mosaics	0.060	0.600	0.540	0.184	0.149
15	Snow and ice	0.001	0.400	0.399	0.025	0.030
16	Barren or sparsely vegetated lands	0.002	0.400	0.398	0.031	0.049
17	Bodies of water	0.002	0.400	0.398	0.039	0.048

higher mean uncertainty interval of 0.55. The reason for this higher level of uncertainty is that there is no direct support for savannas from any of the input data sets.

4.4.3. Sources of uncertainty

By integrating the above analysis and classical evidence theory, we believe that the uncertainties of the final map may have resulted from the following two sources:

- *The uncertainty of input data*. This is an important component of BPA. The errors in land cover classifications are usually expressed using proportional error, which is often difficult to determine (particularly with regard to its spatial distribution). However, we do know that the error of the input data is spatially heterogeneous, even within a specific class. We perform the error of input data at the class level (and even at the data set levels) and using the information in literature reviews in this study, probably, is the most important source of uncertainty in the MICLCover map.
- *The uncertainty of the evidence-generating process*. The relationship between the input data and the decision-making set (i.e., the IGBP land cover types) is another important component of BPA. In general, it is important to obtain sufficiently accurate correlation coefficients between each class of the input data and the IGBP class by inquiring experts in this field. This is another source of uncertainty in the MICLCover map.

5. Summary

An accurate land cover map can significantly reduce the uncertainty of land surface modeling. In this article, a new 1 km land cover map of China, the MICLCover map, was generated with a common classification system (i.e., the IGBP land cover classification

system) by fusing highly accurate land cover information and MODIS2001 map for China. The results of the validation analyses show a great improvement in accuracy in comparison with other land cover maps. For all classes, the MICLCover map provides more spatial details for the distributions of land cover types in the tested locations as compared to other popular land cover products (such as the IGBPDISCover and MODIS2001 products); this is especially true for the cropland, urban, glacier, wetland, and water body classes. For the five provinces examined at local scales, the overall accuracies for forest classes were increased from between 27.77% and 77.89% for the MODIS2001 map to between 42.19% and 88.65% for the MICLCover map. The validation all over China shows that the overall accuracy of the MICLCover map is 71%, which is higher than the accuracies of other land cover maps. The MICLCover map thus has the potential to improve modeling accuracy for land surface processes over China. Additionally, it may support other aspects of land surface science.

From a methodological viewpoint, this study shows that it is effective to produce a new land cover map using the D–S evidence decision rules to fuse multi-source data with different merits as well as different accuracies. In this method, the BPA is the core of the evidence-decision rule for the integration of multi-source class information. The basic probability values of the input data were obtained by combining the literature reviews and expert knowledge. However, there is a need for further research to improve this scheme. A feasible approach is to increase the number of experts to consult in the BPA process. The multiple basic probabilities can be combined using the method of analytical hierarchy process (AHP) to obtain a final basic probability that will serve as input for the combined system. This may reduce the uncertainty in the evidence-generating process. Indeed, the method of error expression for discrete variables is a difficult issue that requires further research. In addition, according to this research and Liu *et al.* (2003b), the integration of new remotely sensed time-series images (such as Envisat MERIS (Medium Resolution Imaging Spectrometer) and MODIS) with other GIS data is a new direction that likely has the potential to improve the accuracy of future land cover mapping.

Acknowledgments

This work is supported by the Chinese Academy of Sciences Action Plan for West Development Project 'Watershed Allied Telemetry Experimental Research (WATER)' (KZCX2-XB2-09), the National Scientific Foundation of China (41001241, 40871190), the National High Technology R&D Program (863) project (grant number: 2009AA122104) and the Research Fund of State Key Laboratory of Resources and Environmental Information System. We thank the guidance of Prof. Jian Ni from the Institute of Botany, Chinese Academy of Sciences for assigning the correlation coefficient between the vegetation classes and IGBP classes, and Prof. Jianhua Wang from the Cold and Arid Regions Environmental and Engineering Research Institute, Chinese Academy of Sciences for assigning the correlation coefficient between the Chinese land use classes and IGBP classes. The China 1:100,000 land use data set was provided by Prof. Jiyuan Liu in the Institute of Geographic Sciences and Natural Resources Research, Chinese Academy of Sciences. We also thank Prof. Liu's enthusiastic help and encouragement. The forest distribution map is supported by the China forest source data center (http://www.cfsdc.org), Chinese Academy of Forestry. The 1:1,000,000 swamp-wetland map was provided by Prof. Shuqing Zhang in the Northeast Institute of Geography and Agroecology, Chinese Academy of Sciences. Generous help for revising the article was also provided by Prof. Yuei-An Liou. We also thank the editor and the anonymous reviewers for their extremely helpful in revising the article.

References

Aspinall, R. and Justice, C., 2003. *A land use and land cover change science strategy* [online]. Washington D.C.: Smithsonian Institution. Available from: http:www.usgcrp.gov/usgcrp/Library/land/LULCCworkshop19-21nov2003.pdf [Accessed 4 November 2009].

Bartholome, E. and Belward, A.S., 2005. GLC2000: a new approach to global land cover mapping from Earth observation data. *International Journal of Remote Sensing*, 26, 1959–1977.

Belward, A.S., eds., 1996. The IGBP-DIS Global 1 km Land Cover Data Set 'DISCover' Proposal and Implementation Plans. *Report of the Land Cover Working Group of IGBP-DIS, IGBP-DIS Working Paper #13*, 11–19. IGBP Data and Information System Office, Toulouse, France.

Bonan, G.B., *et al*., 2002. Landscapes as patches of plant functional types: an integrating concept for climate and ecosystem models. *Global Biogeochemical Cycles*, 16, 1–23.

Bonan, G.B., *et al*., 2003. A dynamic global vegetation model for use with climate models: concepts and description of simulated vegetation dynamics. *Global Change Biology*, 9, 1543–1566.

Cao, G.Z., *et al*., 2009. Fusion of features in multi-temporal SAR imagery to detect changes in urban areas. *International Journal of Remote Sensing*, 30, 5989–6001.

Cayuela, L., *et al*., 2006. Classification of a complex landscape using Dempster-Shafer theory of evidence. *International Journal of Remote Sensing*, 27, 1951–1971.

Cohen, Y. and Shoshany, M., 2005. Analysis of convergent evidence in an evidential reasoning knowledge-based classification. *Remote Sensing of Environment*, 96, 518–528.

Comber, A.J., Law, A.N.R., and Lishman, J.R., 2004. A comparison of Bayes,' Dempster–Shafer and Endorsement theories for managing knowledge uncertainty in the context of land cover monitoring. *Computers, Environment and Urban Systems*, 28, 311–327.

Crutzen, P.J. and Andreae, M.O., 1990. Biomass burning in the tropics – impact on atmospheric chemistry and biogeochemical cycles. *Science*, 250, 1669–1678.

Dai, Y., Zeng, X., and Robert, E., 2001. *Common Land Model (CLM)*. CLM technical documentation and user's Guide, pp. 1–69.

Defries, R.S., *et al*., 1995. Mapping the land surface for global atmosphere-biosphere models: towards continuous distributions of vegetation's functional properties. *Journal of Geophysical Research*, 100, 20867–20882.

Dempster, A.P., 1967. Upper and lower probabilities induced by multivalued mappings. *Annals of Mathematical Statistics*, 38, 325–329.

Friedl, M.A., *et al*., 2002. Global land cover mapping from MODIS: algorithms and early results. *Remote Sensing of Environment*, 83, 287–302.

Gong, P., 2009. The accuracy evaluation for global land cover map based on the global flux site. *Progress in Natural Science*, 19, 754–759.

Gordon, J. and Shortliffe, E.H., 1985. A method for managing evidential reasoning in a hierarchical hypothesis space. *Artificial Intelligence*, 26, 323–357.

Hansen, M.C., *et al*., 2000. Global land cover classification at 1 km spatial resolution using a classification tree approach. *International Journal of Remote Sensing*, 21, 1331–1364.

Hederson-Sellers, A. and Wilson, M.F., 1983. Surface albedo data for climatic modeling. *Review of Geophysics and Space Physics*, 21, 1743–1778.

Hodges, J.C.F., Friedl, M.A., and Strahler, A.H., 2001. The MODIS global land cover product: New data sets for global land surface parameterization. In: *Proceedings of the global change open science conference*. Amsterdam.

Hou, X.Y., eds., 2001. *Vegetation map (1:1,000,000) in China*. Science Press (in Chinese).

Hu, Y.Q., *et al*., 1994. Some achievements in scientific research during HEIFE. *Plateau Meteorology*, 13, 25–236 (in Chinese, English abstract).

IGBP, 1990. *A study of global change in the initial core projects*. Stockholm, Sweden: International Geosphere-Biosphere Programme, *IGBP Global Change Report* No. 12.

Jensen, R., 1996. *Introductory digital image processing: a remote sensing perspective*. 2nd ed. Upper Saddle River, NJ: Prentice Hall, 1–316.

Keller, M., *et al*., 1991. Effects of tropical deforestation on global and regional atmospheric chemistry. *Climatic Change*, 19, 139–158.

Lee, T., Richards, J.A., and Swain, P.H., 1987. Probabilistic and evidential approaches for multisource data analysis. *IEEE Transactions on Geoscience and Remote Sensing*, GE-25, 283–292.

Lei, X.D., *et al*., 2009. Forest inventory in China: status and challenges. *International Forestry Review*, 11, 52–63.

Li, X., *et al*., 2009. Watershed allied telemetry experimental research. *Journal of Geophysical Research*, 114, (D22103), doi:10.1029/2008JD011590.

Liu, J., 1996. *Macro-Scale survey and dynamic study of natural resources and environment of Chinese by remote sensing*. Beijing: Chinese Science and Technology Press, 1–353 (in Chinese).

Liu, J., *et al*., 2002. The land use and land cover change database and its relative studies in China. *Journal of Geographical Sciences*, 12, 275–282.

Liu, J., *et al*., 2005. Spatial and temporal patterns of China's cropland during 1990–2000 an analysis based on Landsat TM data. *Remote Sensing of Environment*, 98, 442–456.

Liu, J., Zhang, Z., and Zhuang, D., 2003a. A study on the spatial – temporal dynamic changes of land – use and driving forces analyses of China in the 1990s. *Geographical Research*, 22, 1–12 (in Chinese).

Liu, J.Y., *et al*., 2003b. Land-cover classification of China: integrated analysis of AVHRR imagery and geophysical data. *International Journal of Remote Sensing*, 24, 2485–2500.

Loveland, T.R., *et al*., 2000. Development of a global land cover characteristics database and IGBP DISCover from 1 km AVHRR data. *International Journal of Remote Sensing*, 21, 1303–1330.

Lu, Y.Z. and Ye, Z.F., 2005. Research on Improved Model of D-S evidence theory. *Computer Engineering and Applications*, 13, 75–77 (in Chinese).

Peddle, D.R., 1995. MERCURY: an evidential reasoning image classifier. *Computers and Geosciences*, 21, 1163–1176.

Rahman, M. and Saha, S., 2008. Multi-resolution segmentation for object-based classification and accuracy assessment for land use/land cover classification using remotely sensed data. *Journal of the Indian Society of Remote Sensing*, 36, 189–201.

Ran, Y., Li, X., and Lu, L., 2010. Evaluation of four remote sensing based land cover products over China. *International Journal of Remote Sensing*, 31, 391–401.

Ronald, E.J., 2003. *IDRISI Kilimanjaro guide to GIS and image processing*. Worcester, MA: Clark University.

Sellers, P.J., *et al*., 1996. A revised land surface parameterization (SiB2) for atmospheric GCMs. Part I: model formulation. *Journal of Climate*, 9, 676–705.

Sellers, P.J., Dickinson, R.E., and Randall, D.A., 1997. Modeling the exchanges of energy, water, and carbon between continents and the atmosphere. *Science*, 275, 502–509.

Shafer, G., 1976. *A mathematical theory of evidence*. Princeton, NJ: Princeton University Press, 1–297.

Shi, Y., 2005, *Concise Chinese glacier directory (fine)*. Shanghai, China: Shanghai Popular Science Press, 1–194 (in Chinese).

Soh, L., Tsatsoulis, C., and Gineris, D., 2004. ARKTOS: An intelligent system for SAR sea ice image classification. *IEEE Transactions on Geoscience and Remote Sensing*, 42, 229–247.

State Forestry Administration, P. R. China., 2004. *National Forest Inventory Technical Regulation*. Beijing, China: State Forestry Administration, 1–68.

Sun, W., *et al*., 2008. Mapping plant functional types from MODIS data using multisource evidential reasoning. *Remote Sensing of Environment*, 112, 1010–1024.

Turner, II, B.L., *et al*., 1995, *Land-use and land-cover change Science/Research Plan*. HDP Report 7/IGBP Report 35, Stockholm and Geneva: Billie Lee Turner II.

Wang, J.M., 1999. Land surface process experiments and interaction study in China – from HEIFE to IMGRASS and GAME-Tibet/TIPEX. *Plateau Meteorology*, 18, 280–294 (in Chinese, English abstract).

Wu, L. and Li, X., 2004. *China glacier information system*. Beijing, China: Ocean Press, 1–135 (in Chinese).

Wu, W.Z., Leung, Y., and Zhang, W.X., 2002. Connections between rough set theory and Dempster–Shafer theory of evidence. *International Journal of General Systems*, 31, 405–430.

Zhang, S., 2002. An introduction of wetland science database in China. *Scientia Geographica Sinica*, 22, 188–189 (in Chinese, English abstract).

Zhu, X., *et al*., 2007. The effects of training samples on the wheat planting area measure accuracy in TM scale (1): the accuracy response of different classifiers to training samples. *Journal of Remote Sensing*, 11, 826–837 (in Chinese, English abstract).